



## ORIGINAL ARTICLE

# Efficient batch and Fixed-Bed sequestration of a basic dye using a novel variant of ordered mesoporous carbon as adsorbent



Asna Mariyam <sup>a</sup>, Jyoti Mittal <sup>a</sup>, Farzeen Sakina <sup>b</sup>, Richard T. Baker <sup>b,\*</sup>,  
Ashok K. Sharma <sup>c</sup>, Alok Mittal <sup>a,\*</sup>

<sup>a</sup> Department of Chemistry, Maulana Azad National Institute of Technology, Bhopal 462 003, India

<sup>b</sup> Department of Chemistry, University of St. Andrews, St. Andrews, Fife KY16 9AJ, United Kingdom

<sup>c</sup> Department of Chemistry, Deenbandhu Chhotu Ram University of Science & Technology, Murthal, Sonapat 131039, India

Received 23 March 2021; accepted 25 April 2021

Available online 30 April 2021

## KEYWORDS

Ordered Mesoporous Carbon;  
Adsorption;  
Film-diffusion;  
Pseudo-second order reaction;  
Fixed-bed

**Abstract** Herein, an ordered mesoporous carbon (OMC) material was prepared using a metal and halogen free method, and its adsorptive potential for the cationic dye, 'Methylene Blue' (MB), was investigated. Batch studies were carried out to determine the influence of pH, dye concentration, adsorbent quantity, and contact time on adsorption behaviour. Adsorption models based on Langmuir, Freundlich, Temkin and Dubinin-Radunkevich isotherms were validated and the thermodynamic variables governing the nature and feasibility of reaction were evaluated. Values of the adsorption uptake at equilibrium ( $q_e$ ) decreased as the temperature was increased, suggesting thereby that the adsorption process involved was exothermic. Kinetic studies indicated that adsorption obeyed pseudo-second order behaviour and operated via a 'film-diffusion' mechanism. When attempts were made to carry out bulk removal of MB using a fixed bed adsorption column, 99.5% saturation could be achieved. Desorption of MB from the used column was performed and dye recovery was almost 100% in the first cycle and on 5th cycle 99% of dye was obtained. This pattern clearly indicates that for the cationic dye MB, OMC acts as a highly efficient and robust adsorbent. © 2021 The Authors. Published by Elsevier B.V. on behalf of King Saud University. This is an open access article under the CC BY-NC-ND license (<http://creativecommons.org/licenses/by-nc-nd/4.0/>).

## 1. Introduction

In recent years ordered mesoporous carbons (OMCs) have become of great interest due to their periodic arrangement of uniform, nano-sized pores, their high specific surface area and tunable pore dimensions (Suib, 2017; Gogotsi, 2015; Zhao et al., 2006). Highly ordered mesoporous structure, high thermal stability, oxidation resistance, along with good electrical and thermal conductivity, are some important properties of the OMC materials. Because of these fascinating properties, OMCs show promise for a wide variety of applications in various

\* Corresponding authors.

E-mail addresses: [rtb5@st-andrews.ac.uk](mailto:rtb5@st-andrews.ac.uk) (R.T. Baker), [aljyomital@gmail.com](mailto:aljyomital@gmail.com) (A. Mittal).

Peer review under responsibility of King Saud University.



Production and hosting by Elsevier

fields and their performance has been found to be superior to other carbon-based porous materials, such as activated carbon (Inagaki et al., 2016; Kado et al., 2014; Inagaki et al., 2014). Amongst the notable potential applications of these materials are components for electrochemical energy storage and conversion, electrochemical sensing, catalysis, gas sensing, optics, and photovoltaics (Eftekhari and Fan, 2017; Ndamaniha and Guo, 2012; Eftekhari, 2017). Lately, the adsorption characteristics of these materials have also been assessed, specifically for removing metal ions, dyes and even gaseous pollutants from wastewater (Liu et al., 2019b; Liu et al., 2019a; An et al., 2020; Tahir et al., 2020; Bhatti et al., 2017; Shoukat et al., 2017; Abdelrahman et al., 2019; Yada et al., 2018).

Many methods have been suggested for the preparation of OMCs (Liang et al., 2008). In one approach, a rather complex multi-step procedure is used in which a carbon precursor is impregnated into a mesoporous template, typically of silica. The precursor is then decomposed and the template dissolved to give the OMC. OMCs may also be prepared directly by the polymerisation – in the presence of an ordered array of self-assembled micelle structures – of organic precursors using inorganic catalysts, such as HCl and Na<sub>2</sub>CO<sub>3</sub>. The first approach, as well as being complex experimentally, often leads to an impure product since it is often impossible to entirely remove the silica. The second, direct method offers a simpler route, but the polymerisation catalysts typically employed can be retained in the product and may be detrimental to the ultimate function of the OMC material.

Recently, the authors developed a method by which they were able to synthesize a series of OMC materials with highly ordered two-dimensional hexagonal pore structures by polymerization of resorcinol and formaldehyde in the presence of ordered assemblies of surfactant micelles. Importantly, this was done with oxalic acid and NH<sub>4</sub>OH as the polymerisation catalysts to avoid retention of any metal or halide ion impurity in the OMC products (Sakina and Baker, 2019). The OMC thus prepared was highly ordered and possessed high specific surface areas (typically 600 m<sup>2</sup>/g) and large specific pore volumes (~0.6 cm<sup>3</sup>/g), and pore diameters of around 7 nm. This OMC has been prepared at up to ~20 g scale. The simplicity of the method employed and the relatively inexpensive reagents used suggest that scale-up to industrial quantities should not meet any serious problems. The material compared favourably with materials prepared by conventional methods (Lu et al., 2008; Ma et al., 2013). Evaluation of the activity of catalysts prepared using this OMC as support also gave encouraging results, and is described elsewhere (Sakina et al., 2020).

In the past two decades adsorption has been established as one of the most reliable techniques for water treatment (Lin, 1993; Cheremisinoff and Angelo, 1980; Bansal et al., 1988; Gorgievski et al., 2013; Bozi et al., 2013; Liu et al., 2021; Kovalakova et al., 2020; Hao et al., 2021). The authors have successfully utilized several novel adsorbents for removal of various environmental pollutants including metal ions and dyes (Mittal et al., 2015; Anastopoulos et al., 2018; Kumar et al., 2020; Mittal et al., 2016; Mittal et al., 2016; Mittal et al., 2016). Adsorption is reliable, versatile and its handling procedures are easy and convenient. The process has the ability to remove both small and bulky organic and inorganic, toxic and non-toxic molecules from their solutions without generating any intermediate products or fragmenting the molecule. In addition, a subsequent desorption process can recover the costly solute molecule without disturbing its structure or affecting its characteristics. For these reasons, adsorption methods have been widely employed for the eradication of a large number of organic and inorganic pollutants and considered better than other physicochemical water purification and wastewater treatment processes such as coagulation, photocatalytic degradation, biochemical degradation etc. (Ruthven, 1984). Since the effectiveness of adsorption depends entirely upon the nature of the adsorbent, researchers are always searching for a material which can prove to be both efficient and economic. It is now well established that reusability of the adsorbent is the prime factor affecting the

viability of the adsorption process (Nayebi et al., 2019). Thus a robust material, which can be used for many adsorption/desorption cycles and remains unaffected even after long-term use, is always desired.

The high specific surface areas and large pore volumes, the uniform, nanoscale pores and the excellent thermal and mechanical stability of OMC make it a very interesting candidate for water treatment by adsorption. OMC prepared free from any metal or halide impurity, using the method of Sakina and Baker (2019) and Sakina et al. (2020), might be expected to exhibit excellent adsorption ability. The present research paper evaluates this material for the adsorption of a representative cationic dye, namely, Methylene Blue (MB), in both batch as well as continuous processes. The dye under study is a well-known toxic colorant and is reported to cause severe health problems in humans, including elevated heart rate, nausea and vomiting, shock, cyanosis, jaundice, quadriplegia, and necrosis of tissue, on acute exposure (Mokhlesi et al., 2003; Harvey and Keitt, 1983; Gillman, 2006).

As far as novelties of the present research paper is concerned, metal and halide free OMC is a recently synthesized material (at one of our research centres) and batch and fixed-bed adsorption of MB over this material is being presented for the first time. Moreover, it is pertinent to note that this is the first reported attempt of adsorption/desorption of MB over fixed-bed adsorbent containing any type of mesoporous carbon.

## 2. Material and methods

### 2.1. Preparation of the OMC

The synthesis of the OMC is described in detail elsewhere (Sakina and Baker, 2019). Briefly, resorcinol and formaldehyde were reacted together in catalysed, staged polymerisation reactions. This was done in the presence of an ordered array of self-assembled micelles comprised of the block co-polymer, Pluronic F127. One novel aspect of the process was the use of the metal- and halogen-free catalysts, NH<sub>4</sub>OH, and oxalic acid in the polymerisation steps. The resulting polymer gel was dried overnight, cured at 80 °C for 24 h and then calcined under flowing under N<sub>2</sub> at 400 °C for 3 h to yield the OMC.

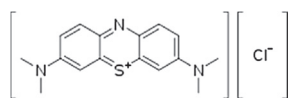
### 2.2. Characterisation of the OMC

The OMC product was characterised using Small Angle (typically  $2\Theta = 0.5 - 5^\circ$ ) X-ray Diffraction (SAXRD), gas physisorption and Transmission Electron Microscopy (TEM). SAXRD diffractograms were obtained by using Cu K $\alpha$  radiation in a PANalytical Empyrean instrument (M/s Malvern Panalytical, UK) operating in reflectance geometry. Gas physisorption isotherms were recorded at liquid N<sub>2</sub> temperature using a Micromeritics TriStar II 3020 instrument (M/s Micromeritics, USA). Degassing of the samples was carried out at 120 °C under vacuum for 12 h or more. The Barrett, Joyner, and Halenda (BJH) pore size distributions were derived from the physisorption data using software supplied with the instrument. Solid-state <sup>13</sup>C NMR spectra were recorded on an Avance III spectrometer (M/s Bruker, Germany) equipped with a 9.4 T wide-bore superconducting magnet (<sup>13</sup>C Larmor frequency of 100.6 MHz). Samples were packed into 4 mm zirconia rotors and spun at the magic angle at a rate of 12.5 kHz. Spectra were recorded with cross polarisation (CP) from <sup>1</sup>H using a spin-lock pulse (ramped for <sup>1</sup>H) of 3.5 ms. Signal averaging was carried out for between 1024

and 10,240 transients with a recycle interval of 5 s. High-power ( $\nu \sim 100$  kHz)  $^1\text{H}$  TPPM-15 decoupling was applied during acquisition. The FT-IR analysis was performed using a IRAffinity-1S instrument (M/s Shimadzu, Japan) with LabSolutions IR software. A background spectrum was taken before each measurement. For TEM, a suspension of the OMC powder in acetone was prepared by ultrasonication and a holey-carbon coated 300 mesh Cu grid was swiped through this using tweezers. Grids were dried overnight under a halogen lamp before examination in the TEM instrument (2011 model, M/s JEOL, Japan) which was equipped with a LaB<sub>6</sub> filament and a digital camera (Multiscan model, M/s Gatan, UK) and operated at 200 kV. Image capture and analysis was performed using the Digital Micrograph software.

### 2.3. Adsorption studies

The IUPAC name of MB (I) is [7-(dimethylamino)phenothiazin-3-ylidene]-dimethylazanium chloride (C<sub>16</sub>H<sub>18</sub>ClN<sub>3</sub>S) and it has a molecular mass of 319.85. It was purchased from Merck, India and was used as received.



(I)

A stock solution ( $1 \times 10^{-2}$  M) of MB was made in aqueous medium and all working solutions were obtained by diluting this with doubly distilled water. Analytical grade reagents, HCl and NaOH were used and these were purchased from M/s Merck, India. To monitor the concentration of dye in batch as well as column adsorption studies a UV-Vis Spectrometer (Model: EI-3375, M/s Electronic India, India) was used. The pH was measured using a computerised pH meter (Model: ESICO-101, M/s ESICO International, India).

#### 2.3.1. Batch studies

In order to perform batch studies, solutions with concentrations of the MB dye of  $1 \times 10^{-5}$  M to  $10 \times 10^{-5}$  M were chosen. 20 ml solution of the known concentration of dye was placed in a 100 ml conical flask with a known quantity of adsorbent and agitated with a mechanical shaker (Model: REMI RSB-12, M/s Remi Sales & Engineering Ltd., India) for a known length of time at an agitation speed of 150 oscillations per minute and at a fixed temperature (30, 40 or 50 °C). The mixture was then separated using a centrifuge (Model: REMI 8C, M/s Remi Sales & Engineering Ltd., India) and the supernatant liquid was decanted. The absorbance of the supernatant was recorded spectrophotometrically at the  $\lambda_{\text{max}}$  of MB 664 nm and the dye uptake was measured.

#### 2.3.2. Column studies

For the continuous removal of the bulk amount of dye the fixed bed adsorber method suggested by Johnston (1972) was used. A slurry of the OMC was prepared (1 g adsorbent in 1000 ml of doubly distilled water) and allowed to stand overnight. It was then slowly fed into a glass column of 30 cm height and 0.5 cm internal diameter using glass wool as a sup-

port. In order to prevent air entrapment, distilled water was run through the glass column before the slurry was added. Thus, the OMC particles settled slowly in the column by progressively displacing the water and a fixed bed of adsorbent was obtained.

Once the uniform fixed bed column was prepared, a solution of known concentration of dye was gradually fed through the adsorbent bed. 10 ml aliquots were collected from the exit of the column and the dye concentration in each sample was measured spectrophotometrically. The concentration of dye in the collected samples increased progressively and dye feeding was stopped when it became equal to the concentration of the dye as initially added.

Retrieval of the adsorbed dye was carried out to test the reusability of the column after complete exhaustion. Dilute HCl was used as the eluent and was passed down the column at a flow rate of 0.5 ml/min. Aliquots were drawn continuously until the dye concentration in the collected aliquots reached zero. At this stage all dye was assumed to have been removed from the column and the desorption procedure was stopped. To examine the column efficiency, the column was reloaded with dye of the same concentration and several adsorption-desorption cycles were carried out.

## 3. Results and discussion

### 3.1. Characterization of the OMC adsorbent

Although the carbonaceous material of the OMC itself is essentially amorphous (since it was calcined at only 400 °C) (Sakina and Baker, 2019), the mesopore structure is ordered enough to give X-ray diffraction peaks at small angles,  $2\Theta$ . The SAXRD pattern of the OMC sample in Fig. 1a shows three clear reflections that can be assigned to the 100, 200 and 210 Miller planes of the pore structure, which consists of a 2-D hexagonal arrangement of parallel cylindrical pores. That is, long, parallel pores, or channels, exist in an arrangement which is hexagonal when these are viewed 'end-on'. The unit cell dimension,  $\mathbf{a}$ , of this 2D hexagonal pore structure can be estimated using trigonometry from the interplanar spacing of the 100 planes,  $\mathbf{d}_{100}$ , (from  $\mathbf{a} = \mathbf{d}_{100}/\cos 30^\circ$ ) and  $\mathbf{d}_{100}$  was obtained using Bragg's Law from the position of the corresponding peak in the SAXRD pattern. The value of  $\mathbf{a}$  was thus found to be 13 nm. The N<sub>2</sub> adsorption and desorption isotherms are presented in Fig. 1b and are indicative of Type IV behaviour in which a sharp capillary condensation step is seen at relative pressure, 0.4–0.8, and with H1 type hysteresis indicating that the mesopores are cylindrical. The specific surface area and specific pore volume derived from these data were  $608 \text{ m}^2\text{g}^{-1}$  and  $0.63 \text{ cm}^3\text{g}^{-1}$ , respectively. The physisorption isotherm data can also be used to determine the pore size distribution and this is presented in Fig. 1c. The sharp, well-defined single peak implies a narrow pore size distribution - that is, that the pore diameters in this sample are very uniform - and that they are centred at a value of 7.0 nm. The  $^{13}\text{C}$  cross-polarization magic angle spinning (CP-MAS) NMR spectrum of the as-prepared OMC material is given in Fig. 2a. Peaks in the figure are labelled and assigned to the various carbon environments shown in the schematic chemical structure of a generic resol unit which is inset in the figure. There is no evidence of retention of the F127 surfactant. Fig. 2b shows the FT-IR

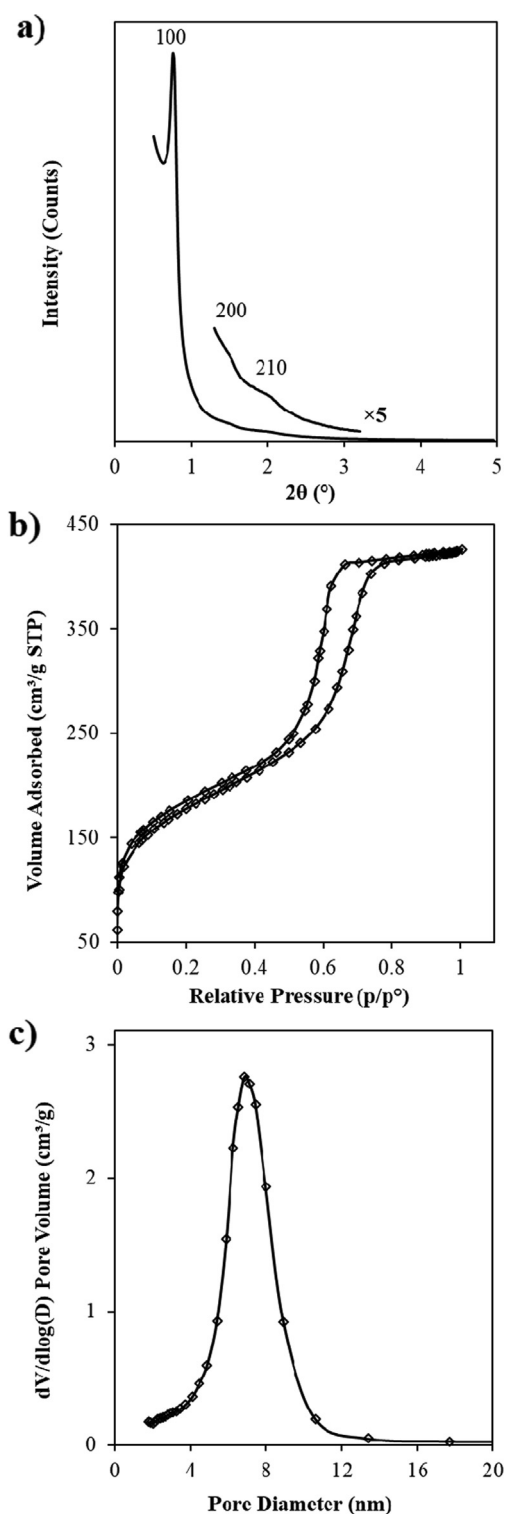


**Fig. 1** Physical characterisation of the as-prepared OMC material: (a) Small angle XRD pattern with Miller indices of main planes indicated; (b) Nitrogen physisorption isotherm; and (c) Pore size distribution derived from the physisorption data.

spectrum of the as-prepared OMC material. The bands between  $1300$  and  $1000\text{ cm}^{-1}$  are assigned to the in-plane bending of the aromatic ring C-H bonds and those at  $1609$  and  $1445\text{ cm}^{-1}$  are due to C-C stretching in the aromatic rings.

Bands around  $1100\text{ cm}^{-1}$  and at  $2868\text{ cm}^{-1}$  correspond, respectively, to the C-O and C-H stretches in the phenolic resin and a weak, broad band around  $3468\text{ cm}^{-1}$  indicates the presence of the OH group. The IR and NMR results indicate that the pore walls of the OMC material would contain aromatic rings, as well as C-H and C-OH functional groups and ether linkages.

Fig. 3 presents typical TEM images at increasing magnification and confirms the findings of the SAXRD and physisorption measurements. Fig. 2a shows the presence of long, parallel cylindrical pores with long-range order. The carbonaceous matrix appears dark and the pores themselves are white. All OMC particles were found to have this structure in TEM. Individual parallel pores are viewed in more detail at higher magnification and 'side-on' in Fig. 3b. In Fig. 3c the hexagonal arrangement of the pores is very clear when these are viewed 'end-on'. By performing a Fourier Transform of this image a Digital Diffraction Pattern (DDP) may be obtained and this is inset in Fig. 3c. The spots in this DDP are labelled with the Miller indices of the corresponding planes of the pore structure. The clarity of this pattern and the sharpness and relative positions of the spots confirms the highly regular, hexagonal arrangement of the mesopores. In the high magnification image in Fig. 1d the hexagonal arrangement of the mesopores is again seen along with the amorphous carbonaceous material forming the pore walls.

### 3.2. Adsorption studies

#### 3.2.1. Effect of pH of solution

In order to assess the influence of pH on the uptake of dye by the adsorbent, studies were performed by varying the pH of the solution from 3 to 10 and results are presented in Fig. 4. Fig. 4 clearly indicates that from pH 3.0 to 7.0 the percentage of dye adsorbed increased from 86 to 100% and then a decrease to 96% was observed at pH 10.0. Since the highest degree of dye removal was recorded at pH 7, all subsequent experiments were performed at this pH only.

The point of zero charge (pHpzc) of the adsorbent OMC, as calculated by the salt addition method, was found to be 6.0. Thus it can be safely interpreted that in environments with pH below 6.0 (pHpzc), i.e. in the acidic media, the surface of the OMC was positively charged ( $\text{pH} < \text{pHpzc}$ ) due to which the extent of adsorption of the cationic dye MB was low. However, above the pHpzc, in the neutral and mildly alkaline media, more adsorption was observed due to establishment of negative charge over the adsorbent surface, increasing thereby the attraction towards the cationic dye and resulting into a higher degree of adsorption of MB. A marginal decrease in adsorption percentage in the more alkaline region (pH 10) may be due to saturation of the available sites on the OMC, and thereby repulsion of MB in solution by the already adsorbed dye molecules. Similar behaviour has also been observed in earlier studies (Mittal, 2006; Zhong et al., 2020; Zhu et al., 2020; Wang et al., 2019).

The presence of hydroxyl groups on the surface of the OMC was confirmed from both FT-IR and  $^{13}\text{C}$  cross-polarization magic angle spinning (CP-MAS) NMR spectra (Fig. 2a & b). MB being a triphenyl thiazine dye can interact with the OMC in the following three ways: (1) electrostatic interaction between the resonating positive charge on the

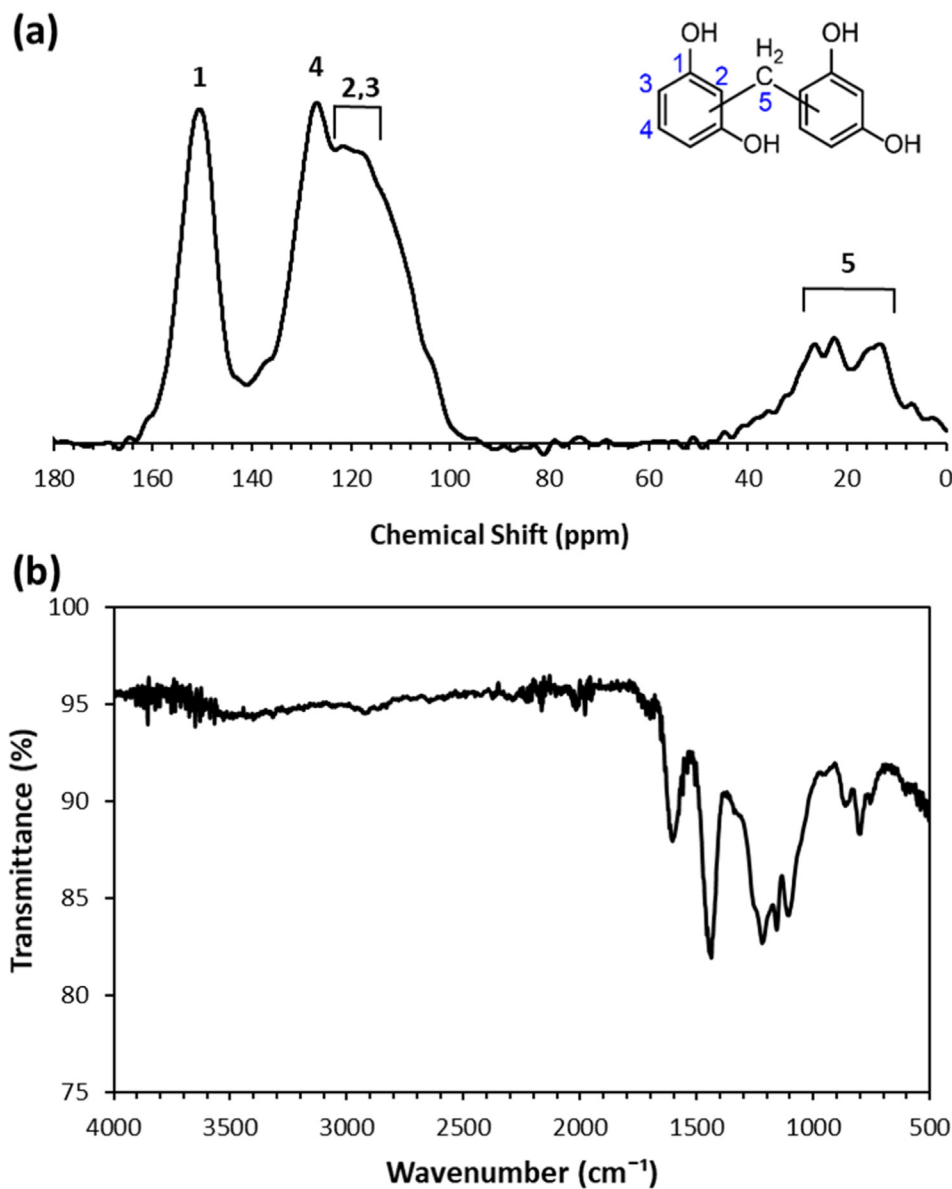


Fig. 2  $^{13}\text{C}$  MAS NMR (a) and FT-IR (b) spectra of the as-prepared OMC material.

N-atom of MB and the deprotonated hydroxyl group; (2) hydrogen-bonding interactions, and (3)  $\pi$ - $\pi$  stacking interactions between the aromatic rings on the OMC (as confirmed by FT-IR) and that of MB. In neutral and alkaline environments, the electrostatic attraction might be the dominant mechanism due to the oppositely charged adsorbate and adsorbent surface.

### 3.2.2. Effect of amount of adsorbent

The selection of the appropriate amount of adsorbent for obtaining maximum adsorption is an important parameter for the batch studies. For this, the extent of adsorption was observed whilst increasing the amount of adsorbent material from 5 to 10 mg in the dye solutions. Dye solutions of the same initial concentration, pH and volume were placed in six different conical flasks and in each flask, a different amount of OMC was added. It was found that as the quantity of the

adsorbent material was increased, the adsorption of the dye – that is, the percentage of dye removal from solution - increased from 82 to 100% (Fig. 5). This increased dye uptake can be explained as being due to the accessibility of more surface sites as the amount of the adsorbent particles was increased. Considering the fact that 10 mg of adsorbent material adsorbs almost 100% of the dye, this amount of adsorbent was used to carry out all further studies.

### 3.2.3. Effect of initial dye concentration

Solutions with the concentration of dye between  $1 \times 10^{-5}$  M and  $1 \times 10^{-4}$  M and each containing 10 mg of OMC were placed in 10 different stoppered conical flasks with other process variables fixed (pH = 7.0; contact time = 2 h; agitation speed = 150 oscillations per minute). Each flask was allowed to shake for a predetermined time interval using a mechanical shaker and dye uptake was recorded. The results obtained are

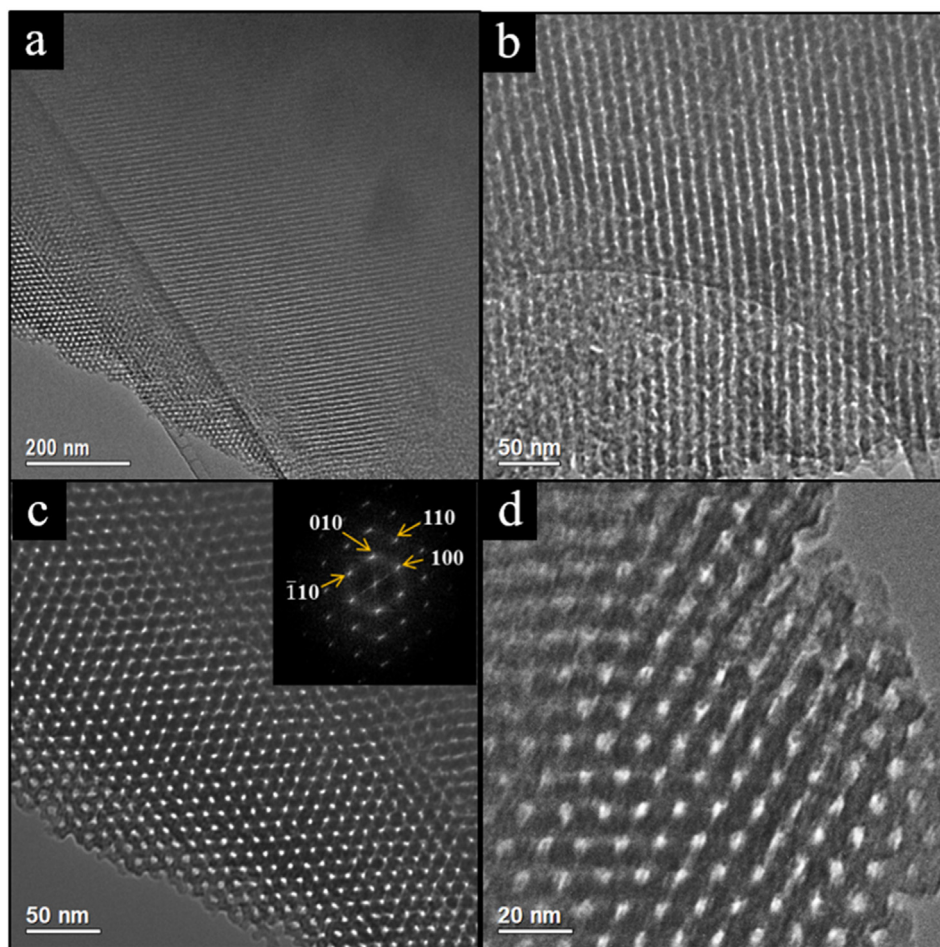


**Fig. 3** TEM Images of the as-prepared OMC material showing: (a) Widespread ordering of pores; (b) Parallel cylindrical pores; (c & d) Hexagonal arrangement of cylindrical pores when viewed “end-on”. The Miller indices of the ordered pore structure are given in the Digital Diffraction Pattern (inset) calculated from the image given in (c).

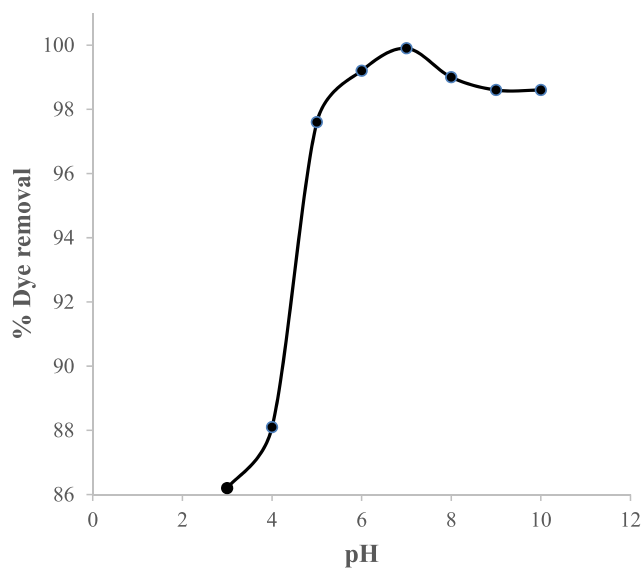


**Fig. 4** Effect of pH on the Adsorption of Methylene Blue over OMC at 30 °C (Dye Concentration =  $5 \times 10^{-5}$  M, Adsorbent Dose = 10 mg/20 ml, Contact Time = 105 min, Agitation Speed = 150 oscillations per minute).

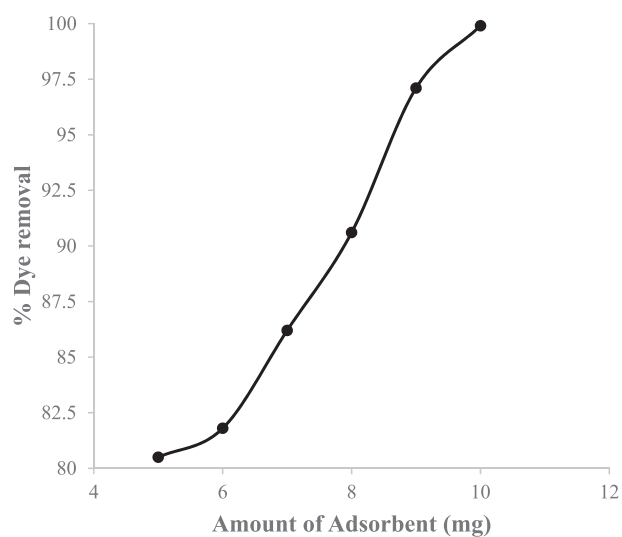


**Fig. 5** Effect of Amount of OMC on the Uptake of Methylene Blue at 30 °C (Dye Concentration =  $5 \times 10^{-5}$  M, pH = 7.0, Contact Time = 105 min, Agitation Speed = 150 oscillations per minute).

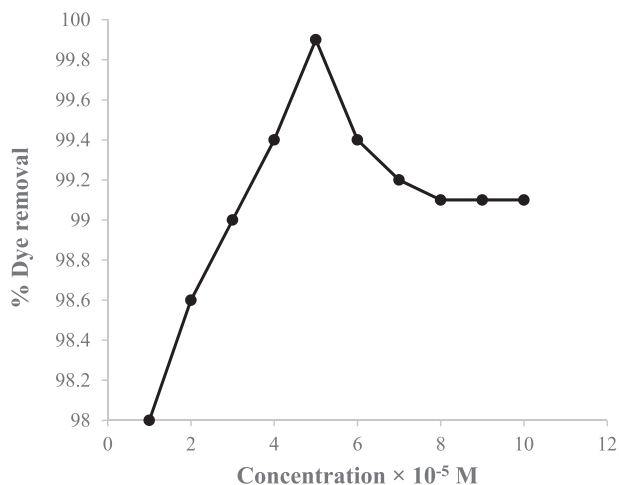


**Fig. 6** Effect of Concentration of Methylene Blue on Adsorption over OMC at 30 °C (pH = 7, Adsorbent Dose = 10 mg/20 ml, Contact Time = 105 min, Agitation Speed = 150 oscillations per minute).

presented in Fig. 6. Fig. 6 shows that the adsorption of the dye on the adsorbent increased from 98 to 100% as dye concentration was increased from  $1 \times 10^{-5}$  M up to  $5 \times 10^{-5}$  M and then slightly decreased to remain almost constant to  $10 \times 10^{-5}$  M. Increase in adsorption with increasing dye concentration is attributed to the increase in the mass driving force between adsorbent particles and adsorbate molecules. It appears that, once the available sites are saturated at  $5 \times 10^{-5}$  M dye concentration, the adsorption of more dye becomes difficult, therefore a plateau is reached. Thus, an MB concentration of  $5 \times 10^{-5}$  M was chosen for use in all other studies.

### 3.2.4. Effect of contact time

The time required to attain equilibrium in the ongoing adsorption process was evaluated by shaking the dye – adsorbent mixture for different time intervals, keeping the pH of the solution, the amount of adsorbent and the dye concentration fixed. The results obtained are given in Fig. 7. It was found that on increasing contact time from 15 min. to 105 min. the adsorption of dye increases from 93% to almost 100%, that after 105 min., equilibrium appears to be established, and that there is then no noteworthy increase in the adsorption of the dye (Fig. 7). Fig. 7 also shows that initially, up to 45 min., the rate of adsorption is quite high and beyond this time for the next hour (till 105 min) uptake of the dye is slower. It can be understood that, during the initial period of adsorption, the dye molecules easily occupy vacant surface sites of the adsorbent resulting in a faster rate of adsorption. However, as adsorption progresses, the number of vacant sites on the adsorbent becomes limiting due to the presence of adsorbate molecules over its surface and once all sites are occupied, adsorption stops and the dye uptake attains a constant value.

### 3.2.5. Adsorption isotherm models

For any adsorption process, the testing of various isothermal adsorption models is an essential component of the methodology as it helps in designing an efficient sorption system. For the present studies, four models, namely the Langmuir,

Freundlich, Temkin and Dubinin-Radunkevich (D-R) adsorption models, were selected and tested against the data. The theory and applications of each of these models have been explained in several books and research publications (Langmuir, 1918; Adamson and Gast, 1997; Masel, 1996).

The Langmuir adsorption model is based on the hypothesis that the uptake of the adsorbate takes place on a homogenous surface by the process of monolayer adsorption, and that there is no interaction between adsorbate ions. The model can be mathematically summarised in the following equation:

$$\frac{1}{q_e} = \frac{1}{q_0} + \frac{1}{bq_0C_e} \quad (1)$$

where,  $q_e$  is the quantity of dye adsorbed ( $\text{mol.g}^{-1}$ ),  $q_0$  is the maximum adsorption capacity per unit mass of adsorbent ( $\text{mol.g}^{-1}$ ),  $b$  is the energy of adsorption ( $\text{J.mol}^{-1}$ ) and  $C_e$  is the equilibrium molar concentration of the dye ( $\text{mol.L}^{-1}$ ).

Based on Eq. (1), typical Langmuir adsorption isotherm graphs were plotted for experimental temperatures of 30, 40 and 50 °C and these are presented in Fig. 8. It is clear that, at each temperature, a linear trend with a regression coefficient close to a value of unity was obtained. This clearly indicates that, at each temperature, adsorption of MB over the OMC followed the Langmuir adsorption isotherm and, therefore, formation of a monolayer of MB with no interaction between its molecules can be inferred. The values of the constants  $b$  and  $q_0$  obtained from the intercepts and slopes of the straight lines are given in Table 1.

A further analysis of the MB-OMC adsorption system was made by employing the Freundlich adsorption model, where it is postulated that the affinities of binding of the adsorbate on the surface of the adsorbent are affected by the interactions between the adsorbed molecules. As a consequence, the sites with the stronger affinities are occupied first. The model helps in diagnosing non-ideal adsorption on heterogeneous surfaces as well as multilayer adsorption. The following mathematical

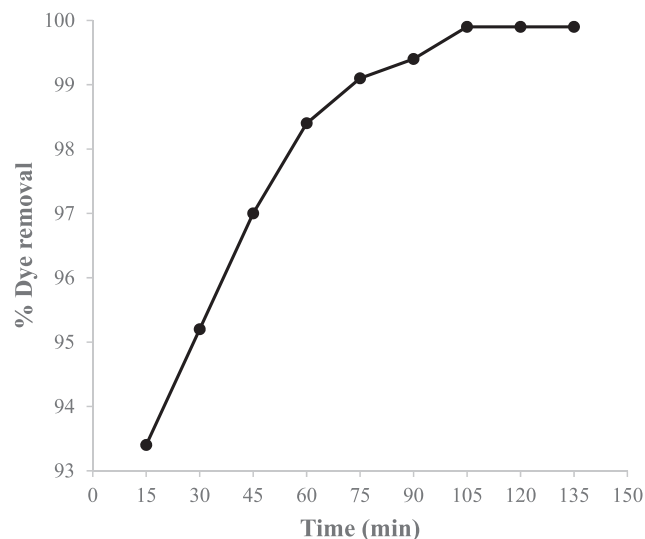


**Fig. 7** Effect of Contact Time on the Uptake of Methylene Blue by OMC at 30 °C (Dye Concentration =  $5 \times 10^{-5}$  M, pH = 7.0, Adsorbent Dose = 10 mg/20 ml, Agitation Speed = 150 oscillations per minute).

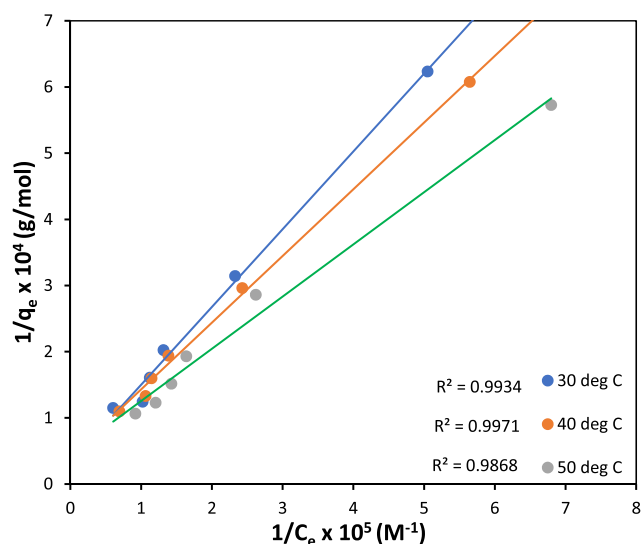


**Fig. 8** Langmuir Adsorption Isotherm for Methylene Blue (pH = 7) – OMC (10 mg/20 ml) System at Different Temperatures (°C).

expression for the Freundlich adsorption isotherm model was applied:

$$\log q_e = \log K_F + \left(\frac{1}{n}\right) \log C_e \quad (2)$$

Where  $q_e$  and  $C_e$  denote the equilibrium concentration and amount adsorbed, respectively, as mentioned above, and  $K_F$  and  $n$  represent the Freundlich constants corresponding to the adsorption capacity and adsorption intensity of the specific adsorbate – adsorbent system, respectively.

The graphs of  $\log q_e$  against  $\log C_e$  at temperatures of 30, 40 and 50 °C are presented in Fig. 9 and linear plots with high regression coefficients were obtained. This clarifies that, after the dye monolayer is homogeneously spread over the adsorbent, adsorption of the dye continues resulting in multilayer formation over the OMC. The values for constants  $K_F$  and  $n$

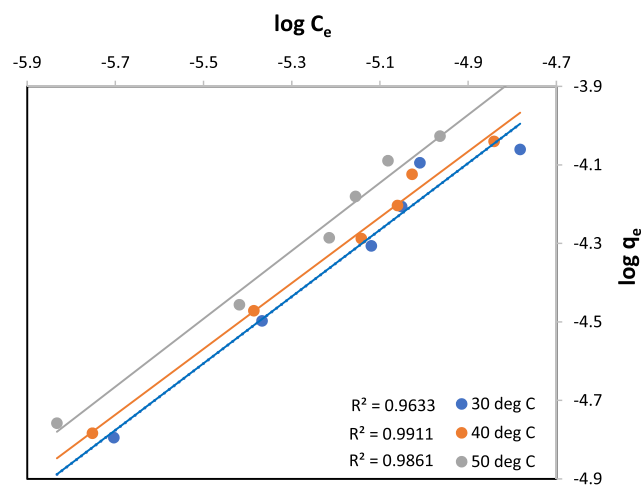


**Fig. 9** Freundlich Adsorption Isotherm for Methylene Blue (pH = 7) – OMC (10 mg/20 ml) System at the Temperatures Indicated (°C).

were determined from the equations of the linear plots and are given in Table 1.

In order to test for the presence of indirect interactions between adsorbate species, the Temkin model was also tested. The linear form of the Temkin isotherm equation is given as:

$$q_e = k_1 \ln k_2 + k_1 \ln C_e \quad (3)$$

where,  $k_1$  is heat of adsorption and equal to  $RT/b$ ,  $R$  (8.314 J.  $K^{-1}mol^{-1}$ ) and  $T$  (in K) have their conventional meanings, and  $k_2$  ( $l.g^{-1}$ ) is the equilibrium binding constant. Graphs of  $q_e$  versus  $\ln C_e$  were plotted at all three temperatures of interest and these are shown in Fig. 10. The linear fits to all three lines have low regression coefficient values. Therefore, the adsorption cannot be considered to obey the Temkin adsorption isotherm model. Nevertheless, the values of Temkin constants are presented in Table 1.

In a further attempt, the DR adsorption model was applied to the experimental data. This is used to obtain an estimate of

**Table 1** Values of Various Adsorption Isotherm Constants for the uptake of Methylene Blue by OMC at Different Temperatures.

Langmuir Constants					
$q_0$ (mmol.g <sup>-1</sup> )			$b \times 10^4$ (l.mol <sup>-1</sup> )		
30 °C	40 °C	50 °C	30 °C	40 °C	50 °C
0.31	0.24	0.21	2.77	4.18	5.91
Freundlich Constants					
$n$			$K_f$		
30 °C	40 °C	50 °C	30 °C	40 °C	50 °C
1.17	1.19	1.15	1.18	1.10	1.86
Temkin Constants					
$k_1$ (l.mol <sup>-1</sup> ) $\times 10^{-5}$			$k_2 \times 10^5$		
30 °C	40 °C	50 °C	30 °C	40 °C	50 °C
4.00	4.00	4.00	2.68	2.68	2.68
D-R Constants					
$X_m$ (mmol.g <sup>-1</sup> )			$\beta \times 10^{-9}$ (mol <sup>2</sup> J <sup>-2</sup> )		
30 °C	40 °C	50 °C	30 °C	40 °C	50 °C
7.02	6.65	8.51	6.00	5.00	5.00

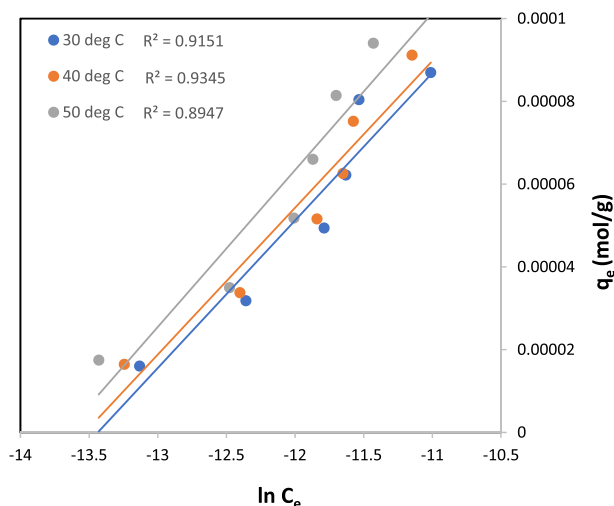


**Fig. 10** Temkin Adsorption Isotherm for Methylene Blue (pH = 7) – OMC (10 mg/20 ml) System at the Temperatures Indicated ( $^{\circ}\text{C}$ ).

the porosity of the adsorbent and the free energy of the adsorption process by use of the relation:

$$\ln q_e = \ln X_m - \beta \epsilon^2 \quad (4)$$

where,  $q_e$  is the quantity of dye adsorbed per unit mass of adsorbent (in  $\text{mol.g}^{-1}$ ),  $X_m$  is the maximum adsorption capacity ( $\text{mol.g}^{-1}$ ),  $\beta$  is the activity coefficient ( $\text{mol}^2.\text{J}^{-2}$ ) linked to the mean adsorption energy and  $\epsilon$  is the Polanyi potential, which is given by:

$$\epsilon = RT \left( 1 + \frac{1}{C_e} \right) \quad (5)$$

where,  $R$  ( $\text{J.mol}^{-1}.\text{K}^{-1}$ ) and  $T$  (K) have their normal meanings and  $C_e$  is the concentration of adsorbate at equilibrium ( $\text{mol.L}^{-1}$ ). Graphs of  $\ln q_e$  versus  $\epsilon^2$  were plotted at 30, 40 and 50  $^{\circ}\text{C}$  and slopes and intercepts were obtained from each straight line (Fig. 11). The values of slope ( $\beta$ ) were further used

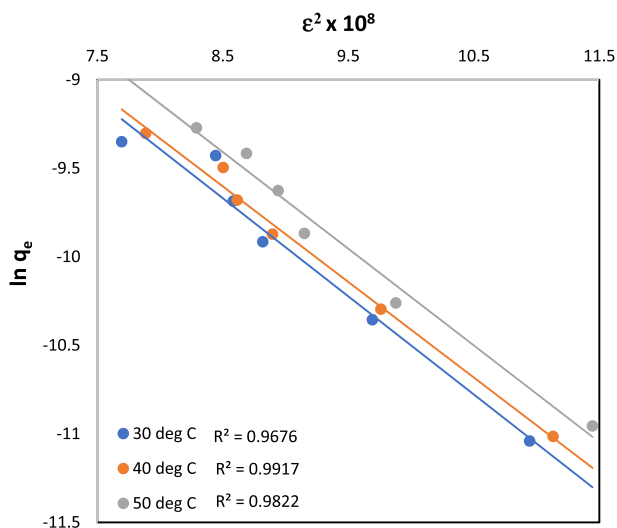


**Fig. 11** D-R Adsorption Isotherm for Methylene Blue (pH = 7) – OMC (10 mg/20 ml) System at the Temperatures Indicated ( $^{\circ}\text{C}$ ).

to calculate mean sorption energy ( $E = 1/\sqrt{-2\beta}$ ). Table 1 presents all the constants obtained from these straight lines.

Interestingly, the DR adsorption isotherm works as a diagnostic tool to distinguish between physisorption and chemisorption processes. It has been postulated that any adsorption system with an ‘E’ value estimated as being less than  $8 \text{ kJ.mol}^{-1}$  follows physisorption, while an ‘E’ value of  $8\text{--}16 \text{ kJ.mol}^{-1}$  confirms chemisorption to be the governing factor of the controlling process (Hutson and Yang, 1997). In the present case, on the basis of the above expressions, values of E were calculated as 9.1, 10 and  $10 \text{ kJ.mol}^{-1}$  at 30, 40 and 50  $^{\circ}\text{C}$ , respectively, indicating thereby the involvement of chemisorption.

### 3.2.6. Evaluation of thermodynamic parameters

One of the important uses of the Langmuir adsorption isotherm model is to calculate various important thermodynamic parameters. The Langmuir constant,  $b$ , refers to energy of adsorption and can be directly used to evaluate the thermodynamic variables relating to the adsorption process such as  $\Delta G^{\circ}$ ,  $\Delta H^{\circ}$  and  $\Delta S^{\circ}$  by following the well-known relations (Adamson and Gast, 1997; Masel, 1996):

$$\Delta G^{\circ} = -RT \ln b \quad (6)$$

$$\Delta H^{\circ} = -R \left( \frac{T_2 T_1}{T_2 - T_1} \right) \times \ln \left( \frac{b_2}{b_1} \right) \quad (7)$$

$$\Delta S^{\circ} = \frac{(\Delta H^{\circ} - \Delta G^{\circ})}{T} \quad (8)$$

where,  $b$ ,  $b_1$  and  $b_2$  are the Langmuir constants ( $\text{L.mol}^{-1}$ ) at different temperatures (K) and  $R$  has its normal meaning ( $\text{J.mol}^{-1}.\text{K}^{-1}$ ).

By using Eqs. (6), (7) and (8),  $\Delta G^{\circ}$ ,  $\Delta H^{\circ}$  and  $\Delta S^{\circ}$  values were determined and these are presented in Table 2. Negative values of  $\Delta G^{\circ}$  at all three experimental temperatures indicate the spontaneity and feasibility of the adsorption process. Negative values of  $\Delta H^{\circ}$  at all three temperatures show that the MB – OMC adsorption process is exothermic. The exothermic nature of the ongoing process can be further verified by observing the decrease in the amount of MB adsorbed at equilibrium with increasing temperature. In addition, the value of  $\Delta G^{\circ}$  decreased with increasing temperature, indicating a greater driving force for adsorption at lower temperatures and this fact is further confirmed by the exothermic nature of the process. The positive values of entropy change,  $\Delta S^{\circ}$ , reflect an increased degree of disorder during adsorption at the solution-solid interface and no significant change in the internal structure of the adsorbent.

Further, as described by Weber and Chakravorti, determining the separation factor ( $r$ ) using the expression,

$$r = \frac{1}{1 + bC_0} \quad (9)$$

where  $b$  is the Langmuir constant ( $\text{L.mol}^{-1}$ ) derived from Eq. (1) and  $C_0$  is the initial dye concentration ( $\text{mol.L}^{-1}$ ), the favourability of the process can be determined (Adamson and Gast, 1997). For  $r > 1$ ,  $r = 1$ , and  $r = 0$ , the process is said to be unfavourable, linear or irreversible, respectively. Thus the condition  $0 \leq r \leq 1$  refers to a favourable process.

**Table 2** Values of Different Thermodynamic Variables for the uptake of Methylene Blue by OMC at the Temperatures Indicated.

Temperature (°C)	$-\Delta G^\circ$ (kJ.mol <sup>-1</sup> )	$-\Delta H^\circ$ (kJ.mol <sup>-1</sup> )	$\Delta S^\circ$ (JK <sup>-1</sup> mol <sup>-1</sup> )	r values
30	25.77	32.39	21.83	0.42
40	27.69	31.79	13.08	0.32
50	29.51	30.77	3.92	0.25

In the present case, values of 'r' as given in Table 2 clearly refer to a favourable process.

### 3.2.7. Kinetic studies

The purpose of kinetic adsorption studies is to determine the effect of various experimental parameters on the rate of adsorption as well as to identify the rate determining step and to ascertain the adsorption mechanism. In the present case, the amount of dye adsorbed on the surface of the adsorbent was monitored at time intervals of 15 min. The kinetic data obtained were fitted to both Lagergren's rate expression (Eq. (10)) and a pseudo-second order rate expression (Eq. (11)) (Ho and McKay, 1999a). It was found that the  $t/q_t$  vs. time plot at all the three temperatures gave best-fit linear plots with regression coefficients equal to unity (Fig. 12); confirmation of the pseudo-second order rate kinetics for the MB – OMC adsorption. The gradient and intercept of the straight lines obtained gave values of adsorption rate constants of  $2.373 \times 10^3$ ,  $2.658 \times 10^3$  and  $3.617 \times 10^3$  g.mol<sup>-1</sup>min<sup>-1</sup> at 30, 40 and 50 °C, respectively. Accordingly, half-lives at 30, 40 and 50 °C were calculated to be 4.212, 3.762 and 2.765 min. This clearly indicates that with rising temperature the rate constant increased and the half-life of the adsorption reaction decreased.

$$\log(q_e - q_t) = \log q_e - \frac{k}{2.303} \times t \quad (10)$$

$$\frac{t}{q_t} = \frac{1}{k_2 q_e^2} + \frac{t}{q_e} \quad (11)$$

The kinetic data were further analysed by the intra-particle diffusion model proposed by Weber and Morris and given by the following expression:

$$q_t = K_{id} t^{0.5} + C_i \quad (12)$$

where  $K_{id}$  (mol.g<sup>-1</sup>.min<sup>-1/2</sup>) is the intra-particle diffusion constant and  $C_i$  is the constant whose value is proportional to the thickness of the boundary layer. As seen in Fig. 13, the non-linear plots of  $q_t$  versus  $t^{0.5}$  at all temperatures did not pass through the origin, thereby indicating that intra-particle diffusion was not the rate-determining step in the adsorption of MB onto the OMC (Unuabonah et al., 2007).

### 3.2.8. Elucidation of mechanism of adsorption

The kinetic data obtained was also used to investigate the rate-determining step of adsorption of MB on OMC by using a conventional mathematical approach proposed by Boyd et al. (1947) and by Reichenberg (1953). If an adsorption process, involving a dye and a porous adsorbent, is minutely observed then three consecutive stages are possible: (1) diffusion of dye molecules from the solution to the adsorbent surface (termed film diffusion); (2) internal diffusion of dye molecules within the pores of the adsorbent (known as particle

diffusion); (3) adsorption of dye molecules on the internal surface of the adsorbent. Crank (1956) explained that stage (3) occurs so fast that it cannot be called a rate-determining step. Hence, in the adsorption system under study, the rate of the process would be limited by either the film diffusion or particle diffusion mechanism and there would only then be three possibilities: (a) rate of external transport < rate of internal transport (particle diffusion), (b) rate of external transport > rate of internal transport (film diffusion), or (c) rate of external transport  $\approx$  rate of internal transport. Case (c) refers to the formation of a liquid film on the solution-solid interface with a concentration gradient sufficient to prevent the transport of adsorbate from the solution to the solid surface at a significant rate.

The sorption dynamics was quantitatively treated using proper boundary conditions and the following formulae were proposed by Reichenberg (195):

$$F = \frac{Q_t}{Q_\infty} \quad (13)$$

$$F = 1 - \frac{6}{\pi^2} \sum_{n=1}^{\infty} \left(\frac{1}{n^2}\right) e^{(-n^2 B_t)} \quad (14)$$

$$B_t = \frac{\pi^2 D_i}{(r_0)^2} = \text{Time constant} \quad (15)$$

where,  $Q_t$  and  $Q_\infty$  are quantities adsorbed after time,  $t$ , and after infinite time, respectively,  $F$  is the fractional degree of attainment of equilibrium at time,  $t$ , and  $n$  is Freundlich constant,  $B_t$  is the time constant,  $D_i$  is the effective diffusion coefficient within the adsorbent phase (cm<sup>2</sup>.s<sup>-1</sup>) and  $r_0$  radius of the adsorbent particle, which is taken to be spherical.

To diagnose the film and particle diffusion mechanism, for each  $F$ -value, a  $B_t$  value was obtained from Reichenberg's table (Reichenberg, 1953) and  $B_t$  vs. time is plotted. If linear plots passing through the origin are obtained, the mechanism is said to be particle diffusion, otherwise film diffusion is assigned (Reichenberg, 1953). In the present case, Fig. 14 clearly indicates that the straight lines obtained at each temperature do not pass through the origin hence the film diffusion mechanism was operative.

Furthermore, the slope of the  $B_t$  vs. time plot gives the values of the effective diffusion coefficient ( $D_i$ ) of the adsorbate at different temperatures (Table 3) and these  $D_i$  values increase with increasing temperature, indicating the increased mobility of dye molecules at higher temperatures. The corresponding graph of  $\ln D_i$  vs. inverse temperature was plotted at all three temperatures and, by using the following expressions, values of  $D_0$ , energy of activation ( $E_a$ ) and entropy change ( $\Delta S^\ddagger$ ) were evaluated (Table 3):

$$D_i = D_0 e^{\left(\frac{E_a}{RT}\right)} \quad (16)$$

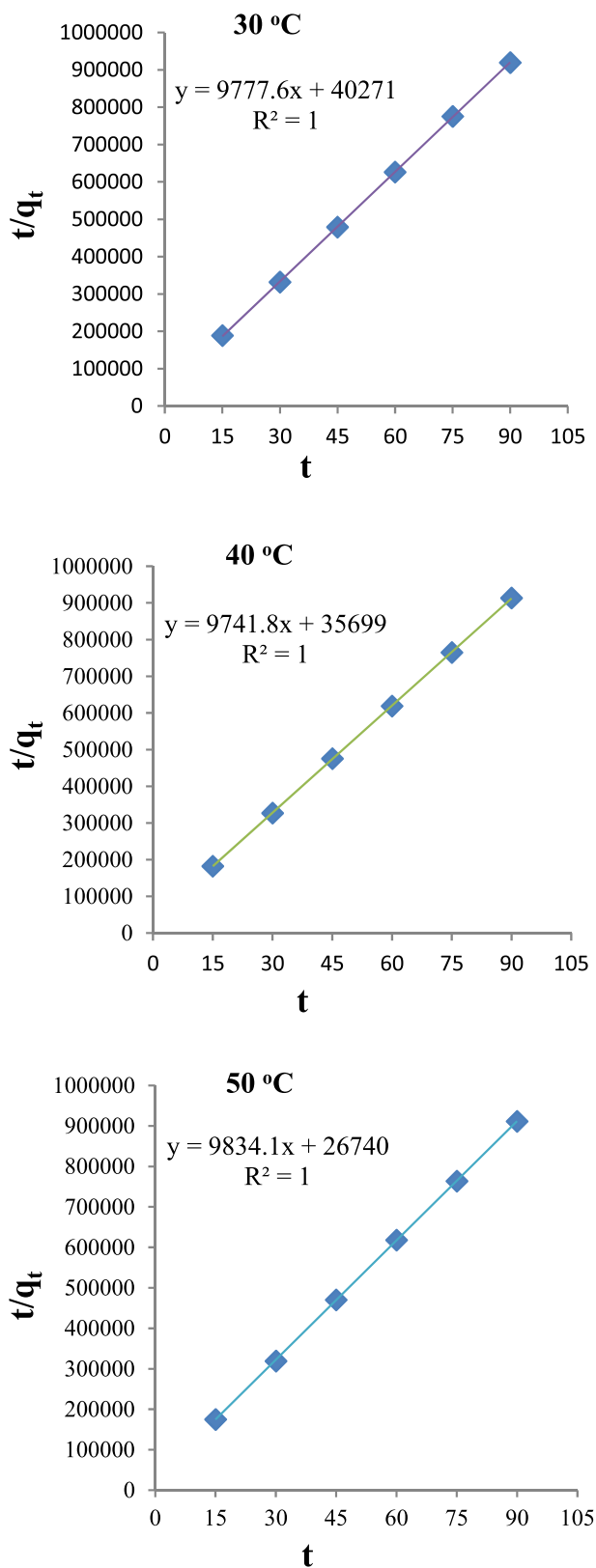


**Fig. 12** Plot of  $t/q_t$  versus Time (mins) for Methylene Blue (pH = 7.0) – OMC (Dose = 10 mg/20 ml) System at Different Temperatures.

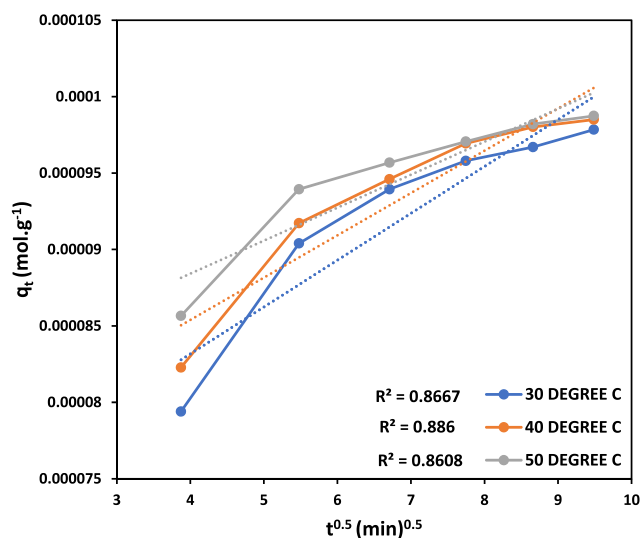


**Fig. 13** Intra-particle diffusion plot of  $q_t$  versus  $t^{0.5}$  for the adsorption of MB onto OMC at 30, 40, and 50 °C.

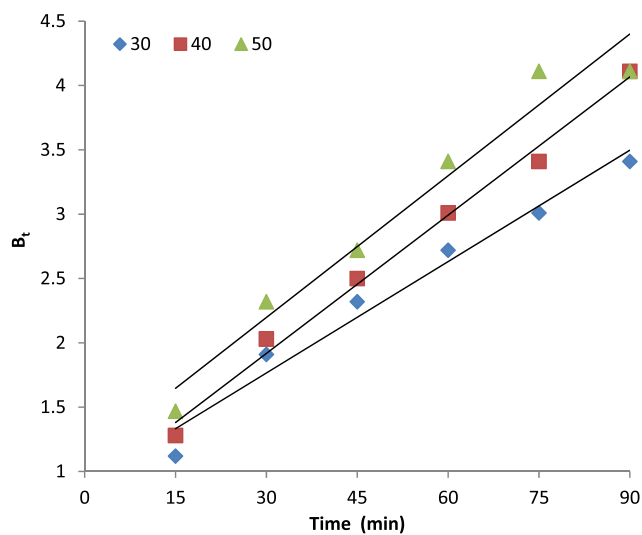


**Fig. 14** Plot of  $B_t$  versus Time for Methylene Blue – OMC Adsorption at Different Temperatures (°C).

$$D_0 = \left( \frac{2.72d^2kT}{h} \right) e^{\frac{E_a}{R}} \quad (17)$$

where,  $D_i$  is the diffusion constant ( $\text{cm}^2/\text{s}$ ),  $D_0$  is the maximum diffusion constant ( $\text{cm}^2/\text{s}$ ),  $E_a$  is the activation energy ( $\text{kJ}\cdot\text{mol}^{-1}$ ),  $R$  and  $T$  have their conventional meanings,  $d$  is the average separation distance ( $\text{cm}$ ) of two neighbouring sites on the adsorbent,  $k$  is the Boltzmann constant ( $1.38 \times 10^{-23} \text{ J}\cdot\text{K}^{-1}$ ), and  $h$  is Planck's constant ( $6.62 \times 10^{-34} \text{ J}\cdot\text{s}$ ).

Table 3 confirms that  $D_i$  increased with increasing temperature. This phenomenon indicates faster diffusion of MB over the surface of OMC at higher temperatures, which may be due to an increase in the mobility of the adsorbing ions over the surface of the OMC. Moreover, with increasing temperature a gradual decrease in the retarding force, acting on the diffusing ions, may also in turn increase the value of  $D_i$ .

**Table 3** Effective Diffusion Coefficient ( $D_i$ ), Pre-Exponential Constant ( $D_0$ ), Activation Energy ( $E_a$ ) and Entropy of Activation ( $\Delta S^\ddagger$ ) for the Diffusion of Methylene Blue over OMC.

$D_i$ ( $\text{m}^2/\text{min}$ )			$D_0$ ( $\text{m}^2/\text{min}$ )	$E_a$ ( $\text{J mol}^{-1}$ )	$\Delta S^\ddagger$ ( $\text{JK}^{-1} \text{mol}^{-1}$ )
30 °C	40 °C	50 °C			
$2.80 \times 10^{-2}$	$3.58 \times 10^{-2}$	$3.67 \times 10^{-2}$	1.0011	$4.988 \times 10^{-3}$	186.616

The low activation energy obtained ( $4.988 \times 10^{-3} \text{ J}\cdot\text{mol}^{-1}$ ) indicates the rapid nature of the adsorption, while positive values of  $\Delta S^\ddagger$  once again confirm increased disorder at the solution-solid interface.

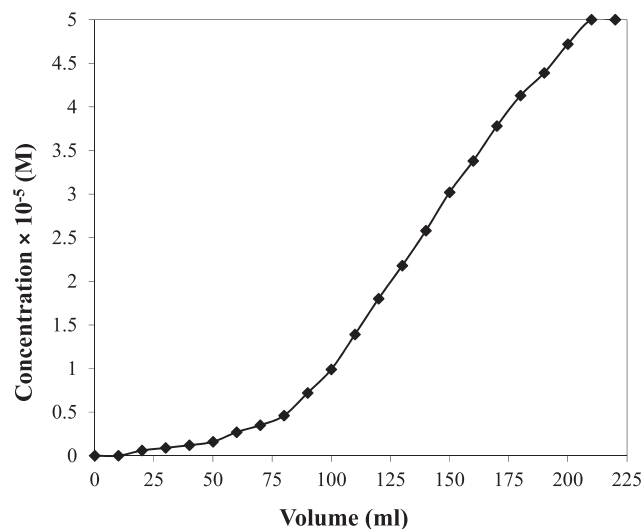
The results obtained in the mass-transfer studies were further verified by applying the mathematical model as proposed by Ho and McKay (1999a) and Ho and McKay (1999b) and graphs of time vs  $\log(1-F)$  were plotted. At all three temperatures, straight lines were obtained which once again confirms the predominance of film diffusion in the adsorption process.

### 3.2.9. Column studies

Though the results obtained above undoubtedly explain the excellent scavenging capacity of OMC, batch processes have limited practical applicability and continuous fixed bed column operations are considered superior. The latter are faster, easier and are able to remove the majority of the adsorbate from the solution. During column operation, the concentration of the adsorbate solution poured into the column remains constant throughout the process, which gives rise to a larger concentration gradient at the adsorbate – adsorbent interface zone. Hence adsorbents exhibit higher exhaustion capacity, resulting in better efficiency than in batch operation (Johnston, 1972).

In the present case, an adsorbent column of 1 g of adsorbent was prepared and dye solution of concentration  $6.5 \times 10^{-4} \text{ M}$  (45.738 mg of dye) of pH 7.0 was allowed to travel through the bed at a flow rate of 0.5 ml/min. Aliquots of 10 ml volume of eluted dye were collected and their dye concentrations were measured. Once the concentration of dye in the aliquots reached  $6.5 \times 10^{-4} \text{ M}$ , the column was assumed to be exhausted and operation was stopped.

The graph of exit concentration of the dye solution versus collected volume of aliquots was plotted and an S-shaped breakthrough curve was obtained (Fig. 15), which can be used to find the adsorption capacity of the prepared column in terms of percentage saturation. In Fig. 15 it can be seen that the exiting eluted solution showed negligible to very small dye concentrations till 6 aliquots (60 ml volume collected) had been taken and after that the dye concentration continuously increased till a plateau was reached at 210 ml of eluent solution collected. This indicates that the maximum rate of adsorption of the dye was attained during the initial stages of operation and that the adsorbent located near the top of the column is saturated first. Thus, a section of uniformly saturated adsorbent bed - i.e. a primary adsorption zone - is formed and this migrates down through the entire adsorbent bed to reach the bottom and after recovering 210 ml the MB concentration in the exiting solution is equal to that of the feed solution, indicating exhaustion of the column. The breakthrough curve (Fig. 15) was analysed to determine various

**Fig. 15** Breakthrough Curve for Adsorption of Methylene Blue over OMC in Column Operations.

parameters by using the following equations (Ho and McKay, 1999b; Michaels, 1952):

$$t_x = \frac{V_x}{F_m} \quad (18)$$

$$t_\delta = \frac{V_x - V_b}{F_m} \quad (19)$$

$$\frac{\delta}{D} = \frac{t_\delta}{t_x - t_f} = \frac{t_\delta}{t_x + t_\delta(f - 1)} = \frac{(V_x - V_b)}{V_b + f(V_x - V_b)} \quad (20)$$

$$f = 1 - \frac{t_f}{t_\delta} = \frac{M_s}{(V_x - V_b)C_0} \quad (21)$$

$$\text{Percentage saturation} = \frac{D + \delta(f - 1)}{D} \times 100 \quad (22)$$

Where,  $\delta$  is length (cm) of the primary adsorption zone,  $t_x$  is total time (min) employed to establish the primary adsorption zone,  $t_\delta$  is the time (min) taken by the primary adsorption zone to percolate its length,  $t_f$  is the time (min) taken for initial adsorption zone formation,  $V_x$  is the volume (ml) corresponding to concentration  $C_x$  i.e the exhaustion point,  $V_b$  is the volume (ml) corresponding to the breakthrough point,  $F_m$  is the mass flow rate (ml/min) of the adsorbent, and  $f$  is the fractional capacity of the column.

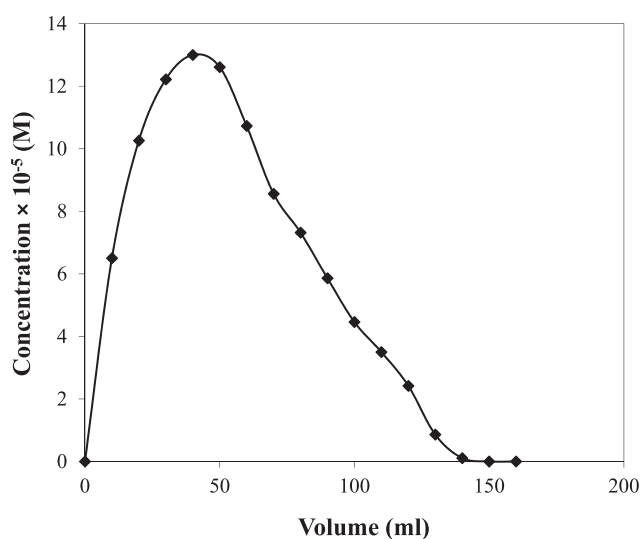
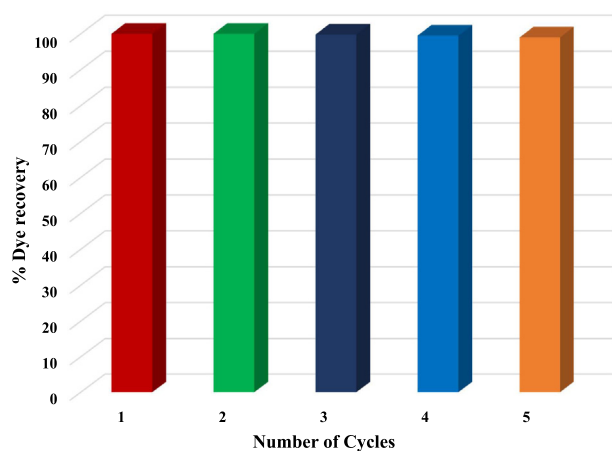
The column parameters calculated using these expressions are presented in Tables 4 and 5. It has been observed that, out of 45.738 mg of eluted MB, 31.477 mg was adsorbed over the OMC and the remaining 14.261 mg was collected in eluent

**Table 4** Calculations of Methylene Blue - OMC Fixed Bed Adsorber Parameters.

$C_o$ (M)	$C_x$ (M)	$C_b$ (M)	$V_x$ (mL)	$V_b$ (mL)	$(V_x - V_b)$ (mL)	$F_m$ (mg/cm <sup>2</sup> )	$D$ (cm)
$6.5 \times 10^{-4}$	$6.5 \times 10^{-4}$	$2.7 \times 10^{-5}$	210	60	150	0.00529	1

**Table 5** Values of Parameters of Methylene Blue - OMC Fixed Bed Adsorber.

$t_x$ (min)	$t_\delta$ (min)	$t_f$ (min)	$f$	$\delta$ (cm)	Percentage Saturation
39,645	28,318	200	0.9929	0.718	99.49

**Fig. 16** Desorption of Methylene Blue from Exhausted Column of OMC.**Fig. 17** Plot of Percentage Dye Recovery versus Number of Adsorption-Desorption Cycles of MB onto OMC.

aliquots. The time needed to establish the primary adsorption zone ( $t_x$ ) was calculated and found to be 39646 min., whereas

the time needed for the primary adsorption zone to transit down the length of the column ( $t_\delta$ ) was 28318 min. The time required for initial formation of the primary adsorption zone ( $t_f$ ) was found to be 100 min. On the basis of these parameters, the degree of saturation of the column was determined to be 99.49%, which once again testifies to the excellent adsorption capacity of the OMC in a neutral medium.

### 3.2.10. Column regeneration and dye recovery

In order to regenerate the used column and to recover the adsorbed MB, dilute HCl with pH 6.0 was passed through the column at a flow rate of 0.5 ml/min. 10 ml aliquots were collected and analysed spectrophotometrically. The graph of collected volume versus dye concentration is presented in Fig. 16. The graph clearly shows that a total of 150 ml of HCl was used to recover 31.4764 (99.999%) of the dye, which, of course, is close to 100% recovery. The graph also indicates that, during addition of the first 50 ml of HCl, almost 55% of the dye was recovered, while 100 ml of HCl gave 93% dye recovery. This essentially complete dye recovery illustrates the excellent desorption ability of the adsorbent.

### 3.2.11. Determination of column efficiency

Efficiency of the column was determined by performing several cycles of adsorption and desorption. In each cycle, the column was loaded with the dye solution of the same concentration and pH ( $6.5 \times 10^{-4}$  M, pH 7.0) and adsorption proceeded till complete exhaustion. To recover the adsorbed dye, dilute HCl was eluted through the exhausted column. To assess the efficiency of the column, a total of five cycles of adsorption and desorption were carried out. It was found that the dye recovery decreased only marginally, and 99% of adsorbed dye could be recovered in the 5th cycle. In the first, second, third, fourth and fifth cycles the recoveries were found to be 100, 100, 99.8, 99.5 and 99.0%, respectively (Fig. 17). The negligible amount of unrecovered dye indicates that the OMC exhibits an excellent adsorption/desorption ability in a neutral medium and can be safely described as a very robust and reversible adsorbent.

## 4. Conclusions

A highly ordered mesoporous carbon of high specific surface area and pore volume was prepared by the polymerization of resorcinol and formaldehyde. Its chemical composition was elucidated using

MAS-NMR and FT-IR methods. Unlike other mesoporous carbons, the OMC thus prepared is free from metal and halide impurities. It exhibited excellent adsorption/desorption performance, specifically for the removal of MB dye from aqueous solution. At pH 7.0, 100% dye adsorption was achieved when  $5 \times 10^{-5}$  M dye remained in contact with 10 mg of OMC for 105 min. The adsorption of MB over the OMC followed both Langmuir and Freundlich adsorption models. On the basis of the DR adsorption isotherm it was confirmed that the ongoing process involves chemisorption. The thermodynamic variables,  $\Delta G^\circ$ ,  $\Delta H^\circ$  and  $\Delta S^\circ$ , of the adsorption system were calculated at three different temperatures and found to be in accordance with existing laws. Adsorption obeyed pseudo-second order rate kinetics and exhibited values of rate constant of  $2.373 \times 10^3$ ,  $2.658 \times 10^3$  and  $3.617 \times 10^3$  g.mole<sup>-1</sup>min<sup>-1</sup> at 30, 40 and 50 °C, respectively. On the basis of models proposed by Reichenberg as well as Ho and McKay, the film diffusion mechanism was seen to be operative in the present case. Bulk removal of the dye was performed in column-based experiments and 99.49% saturation of the column was achieved, while during desorption of the exhausted column almost 100% of the dye was recovered, which demonstrated the excellent adsorption/desorption capacity of the OMC in a neutral medium. The efficiency of the column was also monitored by repeated adsorption/desorption cycles and after the 5th cycle 99% of the adsorbed dye could be recovered. Thus, it can be safely concluded that OMC is an excellent, highly efficient and robust adsorbent for the dye, MB.

### Declaration of Competing Interest

The authors declare that they have no known competing financial interests or personal relationships that could have appeared to influence the work reported in this paper.

### Acknowledgements

The authors are grateful to the Ministry of Human Resource Development of the Government of India for financial support through the SPARC initiative (project: SPARC/2018-2019/P307/SL). We thank the University of St Andrews for a PhD studentship for FS. TEM was carried out at the Electron Microscopy Facility, and NMR at the solid state NMR service, both at the School of Chemistry, University of St Andrews. One of the authors (Asna Mariyam) is thankful to MANIT, Bhopal for providing fellowship support.

### References

Abdelrahman, E.A., Hegazey, R.M., Kotp, Y.H., Alharbi, A., 2019. Facile synthesis of Fe<sub>2</sub>O<sub>3</sub> nanoparticles from Egyptian insecticide cans for efficient photocatalytic degradation of methylene blue and crystal violet dyes. *Spectrochim Acta A Molecular & Biomolecular Spectroscopy* 222,. <https://doi.org/10.1016/j.saa.2019.117195>

Arthur W. Adamson and A.P. Gast (Editors), *Physical Chemistry of Surfaces* (Sixth Edition), Wiley-Interscience (1997).

An, H.J., Park, J.M., Khan, N.A., Jhung, S.H., 2020. Adsorptive removal of bulky dye molecules from water with mesoporous polyaniline-derived carbon. *Beilstein Journal of Nanotechnology* 11, 597–605. <https://doi.org/10.3762/bjnano.11.47>.

Anastopoulos, I., Alok Mittal, M., Usman, Jyoti Mittal, Yu, G., Núñez-Delgado, A., Kornaros, M., 2018. A review on halloysite-based adsorbents to remove pollutants in water and wastewater. *J. Mol. Liq.* 269, 855–868. <https://doi.org/10.1016/j.molliq.2018.08.104>.

Bansal, R.P., Donnet, J.P., Stoeckli, F., 1988. *Active Carbon*. Marcel Dekker, New York.

Bhatti, H.N., Jabeen, A., Iqbal, M., Noreen, S., Naseem, Z., 2017. Adsorptive behavior of rice bran-based composites for malachite green dye: isotherm, kinetic and thermodynamic studies. *J. Mol. Liq.* 237, 322–333. <https://doi.org/10.1016/j.molliq.2017.04.033>.

Boyd, G.E., Adamson, A.W., Meyers, L.S., 1947. The exchange adsorption of ions from aqueous solution by organic zeolites II. *Kinetics. J. Am. Chem. Soc.* 69, 2836–2848.

Bozi, D., Gorgievski, M., Stankovic, V., Strbac, N., Serbula, S., Petrovic, N., 2013. Adsorption of heavy metal ions by beech sawdust – Kinetics, mechanism and equilibrium of the process. *Ecol. Eng.* 58, 202–206. <https://doi.org/10.1016/j.ecoleng.2013.06.033>.

Cheremisinoff, P.N., Angelo, C.M., 1980. Carbon adsorption applications. In: *Carbon Adsorption Handbook*. Ann Arbor Science Publishers Inc, Ann Arbor, MI, p. 1.

Crank, J., 1956. *The Mathematics of Diffusion*. Clarendon press, Oxford.

Eftekhari, A., 2017. Ordered mesoporous materials for lithium-ion batteries. *Microporous Mesoporous Mater.* 243, 355–369. <https://doi.org/10.1016/j.micromeso.2017.02.055>.

Eftekhari, A., Fan, Z., 2017. Ordered mesoporous carbon and its applications for electrochemical energy storage and conversion. *Mater. Chem. Front.* 1, 1001–1027. <https://doi.org/10.1039/c6qm00298f>.

Gillman, P.K., 2006. Methylene blue implicated in potentially fatal serotonin toxicity. *Anaesthesia* 61 (10), 1013–1014. <https://doi.org/10.1111/j.1365-2044.2006.04808.x>.

Gogotsi, Y., 2015. Not just graphene: the wonderful world of carbon and related nanomaterials. *MRS Bull.* 40, 1110–1121. <https://doi.org/10.1557/mrs.2015.272>.

Gorgievski, M., Bozi, D., Stankovic, V., Strbac, N., Serbula, S., 2013. Kinetics, equilibrium and mechanism of Cu<sup>2+</sup>, Ni<sup>2+</sup> and Zn<sup>2+</sup> ions biosorption using wheat straw. *Ecol. Eng.* 58, 113–122. <https://doi.org/10.1016/j.ecoleng.2013.06.025>.

Hao, M., Qiu, M., Yang, H., Hu, B., Wang, X., 2021. Recent advances on preparation and environmental applications of MOF-derived carbons in catalysis. *Sci. Total Environ.* 760,. <https://doi.org/10.1016/j.scitotenv.2020.143333>

Harvey, J.W., Keitt, A.S., 1983. Studies of the efficacy and potential hazards of methylene blue therapy in aniline-induced methaemoglobinemia. *Br. J. Haematol.* 54 (1), 29–41. <https://doi.org/10.1111/j.1365-2141.1983.tb02064.x>.

Ho, Y.S., McKay, G., 1999a. Pseudo-second order model for sorption processes. *Process Biochem.* 34, 451–465. [https://doi.org/10.1016/S0032-9592\(98\)00112-5](https://doi.org/10.1016/S0032-9592(98)00112-5).

Ho, Y.S., McKay, G., 1999b. The sorption of lead (II) ions on peat. *Water Res.* 33, 578–584. [https://doi.org/10.1016/S0043-1354\(98\)00207-3](https://doi.org/10.1016/S0043-1354(98)00207-3).

Hutson, N.D., Yang, R.T., 1997. Theoretical basis for the Dubinin-Radushkevitch (D-R) adsorption isotherm equation. *Adsorption* 3, 189–195. <https://doi.org/10.1007/BF01650130>.

Inagaki, M., Toyoda, M., Tsumura, T., 2014. Control of crystalline structure of porous carbons. *RSC Adv.* 4, 41411–41424. <https://doi.org/10.1039/c4ra06730d>.

Inagaki, M., Toyoda, M., Soneda, Y., Tsujimura, S., Morishita, T., 2016. Templated mesoporous carbons: Synthesis and applications. *Carbon* 107, 448–473. <https://doi.org/10.1016/j.carbon.2016.06.003>.

Johnston, W.A., 1972. *Designing fixed bed adsorbers*. *Chem. Eng.* 79, 87–92.

Kado, Y., Imoto, K., Soneda, Y., Yoshizawa, N., 2014. Highly enhanced capacitance of MgO-templated mesoporous carbons in low temperature ionic liquids. *J. Power Sources* 271, 377–381. <https://doi.org/10.1016/j.jpowsour.2014.08.008>.

Kovalakova, P., Cizmas, L., McDonald, T.J., Marsalek, B., Feng, M., Sharma, V.K., 2020. Occurrence and toxicity of antibiotics in the aquatic environment: A review. *Chemosphere* 251,. <https://doi.org/10.1016/j.chemosphere.2020.126351>

- Kumar, V., Saharan, P., Sharma, A.K., Umar, A., Kaushal, I., Mittal, A., Al-Hadeethi, Y., Rashad, B., 2020. Silver doped manganese oxide-carbon nanotube nanocomposite for enhanced dyesequestration: Isotherm studies and RSM modelling approach. *Ceram. Int.* 46 (8, Part A), 10309–10319. <https://doi.org/10.1016/j.ceramint.2020.01.025>.
- Langmuir, I., 1918. The adsorption of gases on plane surface of glass, mica and platinum. *J. Am. Chem. Soc.* 40 (9), 1361–1402. <https://doi.org/10.1021/ja02242a004>.
- Liang, C., Li, Z., Dai, S., 2008. Mesoporous carbon materials: Synthesis and modification. *Angewandte Chemie International Edition* 47, 3696–3717. <https://doi.org/10.1002/anie.200702046>.
- Lin, S.H., 1993. Adsorption of disperse dye by various adsorbents. *J. Chem. Technol. Biotechnol.* 58, 159–163. <https://doi.org/10.1002/jctb.280580209>.
- Y. Liu, Y. Liu, L. Tang, Y. Zhou, G. Yang, G. Zeng and H. Liu, Mesoporous carbon-based composites for adsorption of heavy metals, Chapter 3 in “Nanohybrid and Nanoporous Materials for Aquatic Pollution Control, Micro & Nano Technologies Series,” L. Tang, Y. Deng, J. Wang, J. Wang and G. Zeng (Editors) Elsevier (2019).
- Y. Liu, Y. Cai, G. Yang, Y. Pang, Y. Zhou, G. Zeng and L. Tang, Mesoporous carbon based composites for removal of recalcitrant pollutants from water, Chapter 2 in “Nanohybrid and Nanoporous Materials for Aquatic Pollution Control, Micro & Nano Technologies Series,” L. Tang, Y. Deng, J. Wang, J. Wang and G. Zeng (Editors) Elsevier (2019).
- Liu, X., Ma, R., Zhuang, L., Hu, B., Chen, J., Liu, X., Wang, X., 2021. Recent developments of doped g-C<sub>3</sub>N<sub>4</sub> photocatalysts for the degradation of organic pollutants. *Critical Reviews in Environmental Science and Technology* 51, 751–790. <https://doi.org/10.1080/10643389.2020.1734433>.
- Lu, A.H., Spliethoff, B., Schüth, F., 2008. Aqueous synthesis of ordered mesoporous carbon via self-assembly catalyzed by amino acid. *Chem. Mater.* 20 (16), 5314–5319. <https://doi.org/10.1021/cm800362g>.
- Ma, T.Y., Liu, L., Yuan, Z.Y., 2013. Direct synthesis of ordered mesoporous carbons. *Chem. Soc. Rev.* 42, 3977–4003. <https://doi.org/10.1039/c2cs35301f>.
- Masel, R., 1996. *Principles of Adsorption and Reaction on Solid Surfaces*. Wiley Interscience.
- Michaels, A.S., 1952. Breakthrough curves in ion-exchange. *Ind. Eng. Chem.* 44, 1922–1930.
- Mittal, A., 2006. Adsorption kinetics of removal of malachite green, from wastewater by hen feathers. *J. Hazard. Mater.* 133 (1–3), 196–202. <https://doi.org/10.1016/j.jhazmat.2005.10.017>.
- Mittal, A., Ahmad, R., Hasan, I., 2016. Biosorption of Pb<sup>2+</sup>, Ni<sup>2+</sup> and Cu<sup>2+</sup> Ions from aqueous solutions by L-Cystein modified montmorillonite immobilized alginate nanocomposite. *Desalin. Water Treat.* 57 (38), 17790–17807. <https://doi.org/10.1080/19443994.2015.1086900>.
- Mittal, A., Teotia, M., Soni, R.K., Mittal, J., 2016. Applications of egg shell and egg shell membrane as adsorbent: A review. *J. Mol. Liq.* 223, 376–387. <https://doi.org/10.1016/j.molliq.2016.08.065>.
- Mittal, A., Ahmad, R., Hasan, I., 2016. Iron oxide-impregnated dextrin nanocomposite: synthesis and its application for the biosorption of Cr (VI) ions from aqueous solution. *Desalin. Water Treat.* 57 (32), 15133–15145. <https://doi.org/10.1080/19443994.2015.1070764>.
- J. Mittal and A. Mittal, Hen Feather, A remarkable adsorbent for dye removal, In: Dr. S.K. Sharma (Ed), Chapter 11 of the Book “Green Chemistry for Dyes Removal from Wastewater” (2015), Publisher: Scrivener Publishing LLC, USA, pp. 409-457.
- Mokhlesi, B., Leikin, J.B., Murray, P., Corbridge, T.C., 2003. Adult toxicology in critical care: Part II: Specific poisonings. *Chest* 123 (3), 897–922. <https://doi.org/10.1378/chest.123.3.897>.
- Nayebi, R., Tarigh, G.D., Shemirani, F., 2019. Porous ionic liquid polymer: A reusable adsorbent with broad operating pH range for speciation of nitrate and nitrite. *Sci. Rep.* 9, 11130 <https://www.nature.com/articles/s41598-019-47648-w>.
- Ndamanisha, J.C., Guo, L.P., 2012. Ordered mesoporous carbon for electrochemical sensing: A review. *Analytica Chimica Acta* 747, 19–28. <https://doi.org/10.1016/j.aca.2012.08.032>.
- Reichenberg, D., 1953. Properties of ion exchange resins in relation to their structure. III. Kinetics of exchange. *J. Am. Chem. Soc.* 75, 589–597.
- Ruthven, Douglas M. (Ed.), 1984. *Principles of Adsorption and Adsorption Processes*. Wiley.
- Sakina, F., Baker, R.T., 2019. Metal- and halogen- free synthesis of ordered mesoporous carbon materials. *Microporous and Mesoporous Materials* 289,. <https://doi.org/10.1016/j.micromeso.2019.109622> 109622.
- Sakina, F., Fernandez-Ruiz, C., Bedia, J., Gomez-Sainero, L., Baker, R.T., 2020. Ordered mesoporous carbon as a support for palladium-based hydridechlorination catalysts. *Catalysts* 11 (1), 23. <https://doi.org/10.3390/catal11010023>.
- Shoukat, S., Bhatti, H.N., Iqbal, M., Noreen, S., 2017. Mango stone biocomposite preparation and application for crystal violet adsorption: a mechanistic study. *Microporous and Mesoporous Materials* 239, 180–189. <https://doi.org/10.1016/j.micromeso.2016.10.004>.
- Suib, S.L., 2017. A Review of recent developments of mesoporous material. *The Chemical Record* 17 (12), 1169–1183. <https://doi.org/10.1002/tcr.201700025>.
- Tahir, M.A., Bhatti, H.N., Hussain, I., Bhatti, I.A., Asghar, M., 2020. Sol-gel synthesis of mesoporous silica-iron composite: Kinetics, equilibrium and thermodynamics studies for the adsorption of Turquoise-Blue X-GB dye. *Zeitschrift für Physikalische Chemie* 234 (2), 233–253. <https://doi.org/10.1515/zpch-2019-1443>.
- Unuabonah, E.I., Adebowale, K.O., Olu-Owolabi, B.I., 2007. Kinetic and thermodynamic studies of the adsorption of lead (II) ions onto phosphate-modified kaolinite clay. *J. Hazard. Mater.* 144 (1–2), 386–395.
- Wang, H., Guo, H., Zhang, N., Chen, Z., Hu, B., Wang, X., 2019. Enhanced photoreduction of U(VI) on C<sub>3</sub>N<sub>4</sub> by Cr(VI) and bisphenol A: ESR, XPS, and EXAFS investigation. *Environmental Science & Technology* 53 (11), 6454–6461.
- Yada, S., Suzuki, T., Hashimoto, S., Yoshimura, T., 2018. Adsorption dynamics of homogeneous polyoxypropylene-polyoxyethylene alkyl ether nonionic surfactants at the air/water interface. *J. Mol. Liq.* 255, 208–214. <https://doi.org/10.1016/j.molliq.2018.01.038>.
- D. Zhao, S. Qiu, Y. Tang and C. Yu (Editors), in: *Recent Progress in Mesostructured Materials: Proceedings of the 5th International Mesostructured Materials Symposium (IMMS2006)*, Shanghai, P. R. China, August 5-7, 2006, Volume 165 *Studies in Surface Science and Catalysis*, Elsevier Science (2007).
- Zhong, X., Lu, Z., Liang, W., Hu, B., 2020. The magnetic covalent organic framework as a platform for high-performance extraction of Cr(VI) and bisphenol a from aqueous solution. *J. Hazard. Mater.* 393,. <https://doi.org/10.1016/j.jhazmat.2020.122353> 122353.
- Zhu, Y., Wang, W., Ni, J., Hu, B., 2020. Cultivation of granules containing anaerobic decolorization and aerobic degradation cultures for the complete mineralization of azo dyes in wastewater. *Chemosphere* 246,. <https://doi.org/10.1016/j.chemosphere.2019.125753> 125753.